Controlled Synthesis and Magnetic Properties of 2D and 3D Iron Azide Networks $_{\infty}^{2}$[Fe(N$_3$)$_2$(4,4′-bpy)] and $_{\infty}^{3}$[Fe(N$_3$)$_2$(4,4′-bpy)]

Aihua Fu,[a, c] Xiaoying Huang,[a] Jing Li,*[a] Tan Yuen,[b] and Chyan Long Lin[b]

Abstract: Controlled synthesis of transition metal complexes with mixed ligands has led to two new compounds with the same empirical formula [Fe(N$_3$)$_2$(4,4′-bpy)] (4,4′-bpy = 4,4′-bipyridine). The compound 2D-[Fe(N$_3$)$_2$(4,4′-bpy)] (**I**) contains end-on (EO) bridging azido ligands. It crystallizes in the orthorhombic crystal system, space group *Cmmm* (No. 65): $a = 11.444(2)$ Å, $b = 15.181(3)$ Å, $c = 3.458(1)$ Å, $V = 600.8(2)$ Å^3, and $Z = 2$. The compound 3D-[Fe(N$_3$)$_2$(4,4′-bpy)] (**II**) contains end-to-end (EE) azido bridges. It belongs to the tetragonal crystal system, space group $P4_12_12$ (No. 92): $a = 8.132(1)$ Å, $b = 8.132(1)$ Å, $c = 16.708(3)$ Å, $V = 1104.9(5)$ Å^3, and $Z = 4$. Crystals of **I** and **II** have been grown by the diffusion method. Phase-pure samples of both compounds have been obtained by means of an optimal solution synthesis. Spontaneous long-range magnetic ordering was found in both **I** and **II**, with **I** being a metamagnet, and **II** being a ferromagnet. For **I**, in the low-field region, multiple transitions at $T_{N1} = 20$ K and $T_{N2} = 5$ K were observed, and these indicated the existence of Fe moment reorientation. Heat capacity measurements on **II** confirmed ferromagnetic transition at $T_C = 20$ K.

Keywords: controlled synthesis · iron · magnetic properties · polymers

Introduction

A significant amount of research has been dedicated to the study of molecular-based magnets, the structures of which are built upon inorganic motifs bridged by organic components.[1] In the light of controlled synthesis, we have recently proposed and successfully prepared a group of two-dimensional layered networks based on six-coordinate, divalent metal centers, [M(ox)(4,4′-bpy)] (M = Fe, Co, Ni, Zn; ox = $C_2O_4^{2-}$, 4,4′-bpy = 4,4′-bipyridine) and [MCl$_2$(4,4′-bpy)] (M = Fe, Co, Ni, Co/Ni).[2] In these structures, metal centers are bonded by a μ_2-bridging ligand, L, to form one-dimensional magnetic chains, as illustrated in Figure 1 (left). A second, lengthier and rigid bridging ligand, such as 4,4′-bpy (approx. length: $\approx$7.1 Å), is used to complete the metal coordination and to interconnect the parallel chains, which generates a two-dimensional network structure. The intrachain metal–metal interactions constitute the primary cause for the magnetic ordering in these compounds, whereas interchain interactions are usually secondary. Evidently, the magnetic properties are directly affected by the nature of the bridging ligand, L. While comparisons have been made between the two structures, with L being $C_2O_4^{2-}$ and Cl^-, from which some interesting conclusions have been derived, the two ligands are quite different in a number of ways. Synthesis of related structures containing ligands (L) with similar properties and bonding nature would therefore be of great value for understanding the ligand effect on the magnetic interactions and the structure–property correlation.

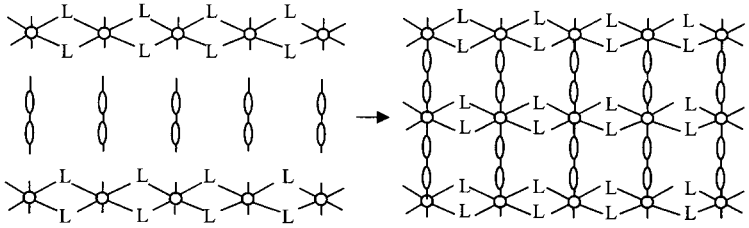

Figure 1. One-dimensional magnetic chains of ML$_2$ (left, M = metal center, L = μ_2 ligand) are interconnected by another rigid and lenthier ligand to form a two-dimensional crystal structure (right).

The investigation of transition metal azide coordination complexes has become an area of increasing interest. This is primarily due to the versatility of the azido ligand in the self-

[a] Prof. J. Li, A. Fu, X. Huang
Department of Chemistry, Rutgers University, Camden
New Jersey 08102 (USA)
Fax: (+1) 856-225-6506
E-mail: jingli@crab.rutgers.edu

[b] Prof. T. Yuen, Prof. C. L. Lin
Department of Physics, Temple University, Philadelphia
Pennsylvania 19122 (USA)

[c] A. Fu
Current address: Department of Chemistry
University of California, Berkeley, CA 94720 (USA)

  0947-6539/02/0810-2239 $ 20.00+.50/0

assembly of extended networks and interesting magnetic properties exhibited by these compounds. μ-(1,1)(EO),[3] μ-(1,3)(EE),[4] μ-(1,1,1),[5] μ-(1,1,3),[6] alternating μ-(1,1), and μ-(1,3) in the same structure[7] and monodentate μ-(1)[8] are among the various coordination modes of the azido ligand that have been reported. Such a coordination versatility has not only resulted in a variety of crystal structures of zero, one, two, and three dimensions, but also the tuning of magnetic properties of these compounds by adjusting the relative positions of metal atoms and the exchange coupling parameter J.[4a, b, 7a–d, 8b] It has been noted that the induced magnetic orderings are ferromagnetic when bridging azido ligands are in μ-(1,1) mode with small bridging angles (e.g. less than 108° for Cu,[7e] but antiferromagnetic when the coordination mode of the azido ligands is μ-(1,3) or μ-(1,1) with big bridging angles.[9] Since N_3^- is an excellent coordinating ligand in mediating magnetic exchange coupling, a one-dimensional magnetically active network with a two-dimensional crystal structure similar to $[MCl_2(4,4'\text{-bpy})]$ is anticipated if Cl^- can be replaced by this pseudo-halide ion. This would allow us to investigate the effect of the similar ligands on the magnetic properties of the $[ML_2(4,4'\text{-bpy})]$ type structure.

In this work, we present the controlled synthesis, crystal structures, and magnetic properties of 2D-$[Fe(N_3)_2(4,4'\text{-bpy})]$ (**I**) and 3D-$[Fe(N_3)_2(4,4'\text{-bpy})]$ (**II**). The two polymorphic phases contain N_3^- azido ions with different coordination modes. They are end-on (EO) in **I**, and end-to-end (EE) in **II**. While 2D-$[Fe(N_3)_2(4,4'\text{-bpy})]$ (**I**) represents a new member of the $[ML_2(4,4'\text{-bpy})]$ family, 3D-$[Fe(N_3)_2(4,4'\text{-bpy})]$ (**II**) crystallizes in a very different structure type. It is also worth mentioning that optimized experimental conditions were achieved, which allowed a total isolation of phase-pure samples of the two compounds. The magnetic and heat capacity measurements have revealed very interesting magnetic behavior of the two: while intrachain coupling (along the c direction) of Fe^{2+} is positive, 2D-$[Fe(N_3)_2(4,4'\text{-bpy})]$ (**I**) orders antiferromagnetically below 20 K, due to the negative interchain coupling. Also a metamagnetic transition occurs around a critical field of 25 kG for $T = 2$ K. For 3D-$[Fe(N_3)_2(4,4'\text{-bpy})]$ (**II**), the $Fe^{2+}-Fe^{2+}$ coupling is negative at high temperature, but changed to positive below 31 K. The system orders ferromagnetically with a transition temperature of $T_C = 20$ K.

Results and Discussion

Synthesis: Rational control in the construction of extended networks remains a great challenge in crystal engineering. Low-temperature synthesis is favored to preserve the structural units from the reactants to the products.[10] In the preparation of the title compounds, we employed both room-temperature diffusion techniques and solution synthesis. Slow diffusion allowed the development of a different predisposition of metal atoms and ligands in the bond forming process of the extended crystal motifs. Hence, high-quality crystals of both **I** and **II**, suitable for single-crystal X-ray diffraction analysis, were obtained in the same diffusion tube. Initial trial solution synthesis involved aqueous solutions of iron(II) salts and NaN_3, as well as a solution of 4,4′-bpy in methanol. This resulted in a mixture of polycrystalline **I** and **II**. The optimum conditions for generating pure products of **I** and **II** were found by direct reaction of metal ions and ligands under different conditions. Compound **I** was isolated as a single product when an aqueous solution of NaN_3 was added quickly to a mixture of a solution of 4,4′-bpy in methanol and an aqueous solution of $FeCl_2 \cdot 4H_2O$. Single-phase polycrystalline **II** was obtained by slowly mixing of a solution of 4,4′-bpy in methanol, followed by dropwise addition of an aqueous solution of NaN_3 to a stirred aqueous solution of an iron(II) salt. The mixture was then continuously stirred for three hours. Figure 2 shows the X-ray powder diffraction patterns of the two phases, compared with those calculated from single-crystal X-ray diffraction data.

As a pseudo-halide ion, N_3^- may use either an end-on (EO) or an end-to-end (EE) bonding mode to form two-dimensional structures. Structure **1**, which is very similar to that of $[ML_2(4,4'\text{-bpy})]$ ($L = \frac{1}{2}C_2O_4^{2-}$, Cl^-),[2] was formed with an

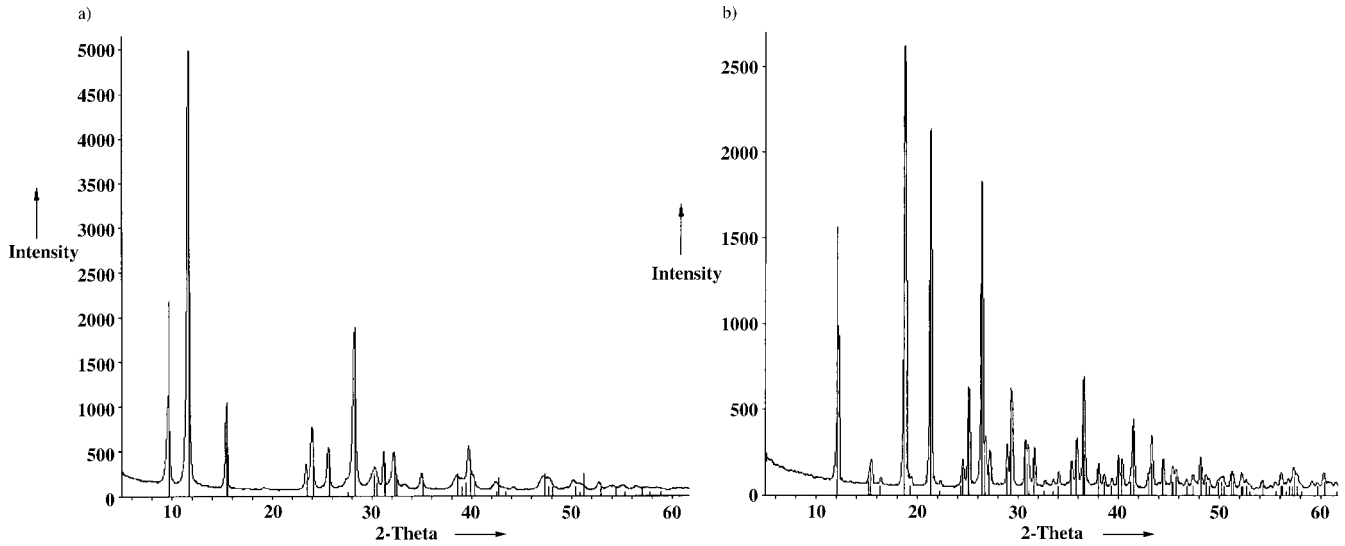

Figure 2. Experimental and calculated powder X-ray diffraction patterns for a) 2D-$[Fe(N_3)_2(4,4'\text{-bpy})]$ (**I**) and b) 3D-$[Fe(N_3)_2(4,4'\text{-bpy})]$ (**II**).

0947-6539/02/0810-2240 $ 20.00+.50/0 *Chem. Eur. J.* **2002**, *8*, No. 10

exclusive EO (or μ-(1,1)) coordination mode of N_3^-, in which all three N atoms of the N_3^- ligands direct outwards from the Fe(bpy) layer. The geometric arrangement of this 2D structure is quite stable. However, when adopting an EE mode, all N atoms were forced into the layer creating a severe steric problem, and consequently an instable structure. Two adaptations to decrease the steric hindrance and maintain a 2D-structure motif were reported in similar systems. First, in the case of $[Cd(SCN)_2(4,4'\text{-bpy})]_n$, the SCN^- ligand adopts an extremely bent shape with torsion angles of 93.7° for Cd–S–C and 139.3° for Cd–N–C. This positions the three atoms, S, C, and N, further away from the metal layer.[11] Second, in the series of $[M(\mu\text{-}(1,3)\text{-}N_3)_2(bpa)]$ (M = Mn, Co, Ni, bpa = 1,2-bis(4-pyridyl)-ethane),[12] which contains a longer and more flexible bidentate ligand, bpa, the 2D structure was stabilized by increasing the metal distance through the bpa bridges, and by a significant twisting of bpa (67° dihedral angle between the two pyridyl rings). Conversely, in the case of $[Fe(\mu\text{-}(1,3)\text{-}N_3)_2(4,4'\text{-bpy})]$ (**II**), neither the tighter ligand, N_3^-, nor the more rigid ligand, 4,4′-bpy, could provide adequate stabilizing functions through the aforementioned geometric distortions. The 2D structure had to break down, and consequently the 3D structure of compound **II** was formed. Similar decompositions, due to changing bonding modes of azido ligands, have been reported.[13]

The following chart illustrates the synthesis and structural relationship based on the above discussions.

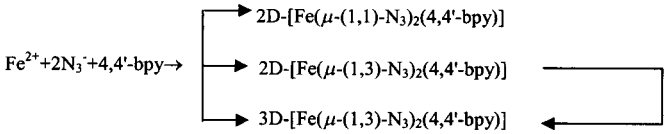

Structures: The crystal structure of compound **I** consists of two-dimensional $[Fe(N_3)_2(4,4'\text{-bpy})]$ layers parallel to the crystallographic *ac* plane. Its three-dimensional structure is completed by stacking these layers on top of each other with a shift of $\frac{1}{2}a + \frac{1}{2}c$ between the adjacent layers (Figure 3). All Fe atoms are octahedrally coordinated with four μ-(1,1) azide ligands in the equatorial plane and two 4,4′-bpy molecules at the axial sites. The Fe–N_{azide} bond length is 2.208(6) Å, and the distance between Fe and $N_{4,4'\text{-bpy}}$ is 2.192(11) Å, comparable with Fe–N bond lengths in the previously reported coordination compounds.[14] The octahedral geometry around each Fe atom is slightly distorted through axial contraction and equatorial distortion. For each 4,4′-bpy ligand, the two pyridyl rings are coplanar and lie in the crystallographic *ab* plane. The terminal nitrogen of the azido ligand is disordered. The N–N–N angle in an azide is 160(3)°. All angles of N_{bpy}–Fe–N_{azide} are 90°. However, there are two different angles for N_{azide}–Fe–N_{azide}, 76.9(4) and 103.1(4)°, respectively. The bridging angle of Fe–N_{azide}–Fe is 103.1(4)°. The Fe–Fe distances are 3.462 Å between the azido-bridged Fe atoms, and 11.430 Å along the Fe–bpy one-dimensional chains, respectively.

Compound **II** has a three-dimensional structure, with each Fe atom bonded to four μ-(1,3) azido ligands and two 4,4′-bpy ligands in the *trans* position (Figure 4). The two pyridyl rings in each 4,4′-bpy ligand are not coplanar, and the dihedral angle is ≈31.3(2)°. The three N atoms from the same azido ligand are nearly linear (N–N–N = 176.8(5)°). Each Fe atom lies on a crystallographic twofold axis that also passes the two N atoms of each 4,4′-bpy ligand. There are two different Fe–N_{bpy} bond lengths, 2.188(4) Å for Fe–N1, and 2.230(4) Å for Fe–$N2^{iv}$. The bond lengths between Fe–N_{azide} are 2.160(4) Å for Fe–$N5^{ii}$ and Fe–$N5^{iii}$, and 2.136(4) Å for Fe–N3 and Fe–$N3^{i}$. These bond lengths are asymmetric due to the prohibition of a crystallographic inversion center in the $P4_12_12$ crystal system, which is also reflected from the nonequivalence of bond angles. All angles of N_{bpy}–Fe–N_{azide} are around 90°. The angles of N_{azide}–Fe–N_{azide} are 91.11(15)° for $N3^{i}$–Fe–$N5^{ii}$ and N3–Fe–$N5^{iii}$ and 88.89(15)° for N3–Fe–$N5^{ii}$ and $N3^{i}$–Fe–$N5^{iii}$. The Fe–N_{azide}–N_{azide} angles are 153.0(4)° for Fe^{vi}–N4–N5 and 128.1(3)° for Fe–N3–N4. The dihedral angle between the Fe–N3–N4–N5 and Fe^{vi}–N5–N4–N3 planes plays an important role in the magnetic properties of related compounds.[15] This angle is 75.62° in **II**. The Fe–Fe distance is 5.867 Å through all EE azido bridges and 11.50 Å when separated by 4,4′-bpy ligands. The structural features presented in **II** compare well with the isostructural compound $[Mn(N_3)_2(4,4'\text{-bpy})]$.[16] Strong $\pi-\pi$ interactions between the pyridyl rings of 4,4′-bpy may be anticipated in **II**. Figure 5 shows the 4,4′-bpy ligands within a

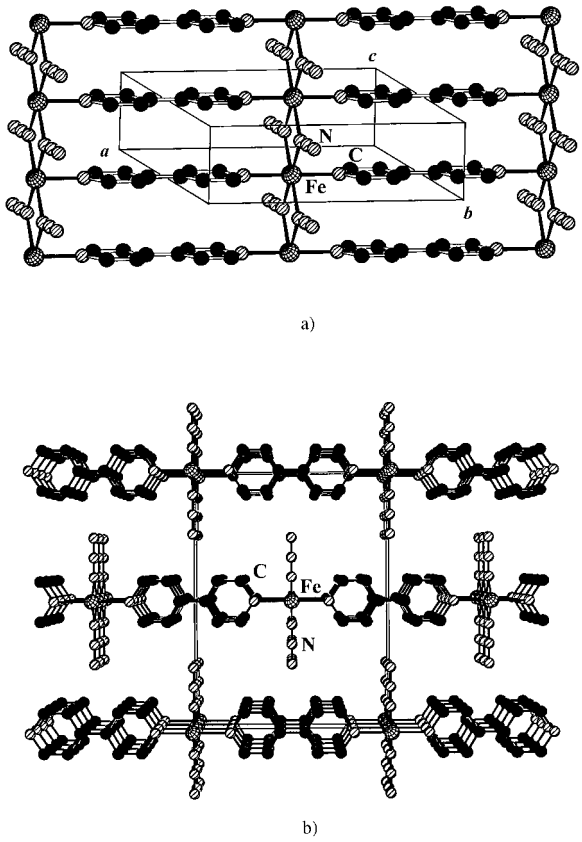

Figure 3. Two-dimensional network of $[Fe(N_3)_2(4,4'\text{-bpy})]$ (**I**): a) view showing a single layer projected along the *b* axis; b) the 2D layers of $[Fe(N_3)_2(4,4'\text{-bpy})]$ (**I**) stacked in a staggered fashion along the *b* axis. The cross-shaded circles are Fe, solid circles are C, single-shaded circles are N.

portion of the structure. The dotted lines connect the atoms from adjacent pyridyl rings. These distances range from 3.6 to 3.8 Å, and are therefore highly subject to $\pi-\pi$ interactions.

Magnetic properties: In Figure 6, the low-temperature portion of χT data for **I** is plotted, measured under several fields. The anomalies observed in χT data of 50 G and 1 kG suggest that spontaneous antiferromagnetic ordering of Fe^{2+} and Fe^{2+} moment reorientations exists in this compound. As reflected in the ZFC (zero-field-cooled) χT of 50 G, the transition temperatures are $T_{N1}=20$ K, $T_{N2}=5$ K, and possibly a third between T_{N1} and T_{N2} at about $T_3=7$ K. However, in ZFC χT of 1 kG, only the anomaly at T_{N2} is readily apparent, while in χT of 10 kG, none of the anomalies appear. In the temperature range of 100 to 350 K, the χT data were fit to the Curie–Weiss law, $\chi T=C/(T+\theta)$. The fitted effective magnetic moment and the Curie–Weiss temperature were $\mu_{eff}=5.2\mu_B$ and $\theta=+45$ K, respectively. The positive θ value indicates a dominant positive interaction between Fe^{2+} ions in this compound, presumably through the one-dimensional Fe–2N_3–Fe chain along the c direction. The interchain interactions of Fe^{2+} are supposedly negative, which lead to the three-dimensional long-range antiferromagnetic ordering.

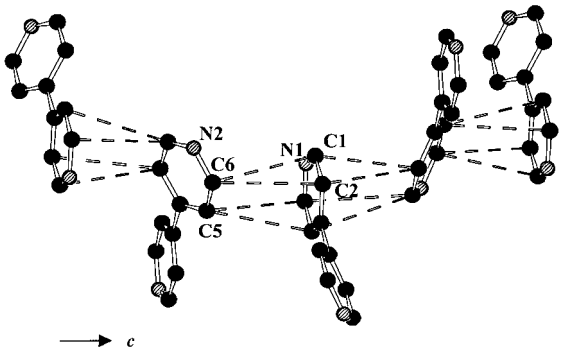

Figure 5. Structural fragment showing the neighboring pyridyl rings of 4,4′-bpy in 3D-[Fe(N_3)$_2$(4,4′-bpy)] (**II**). Dotted lines indicate distances between 3.6 and 3.8 Å.

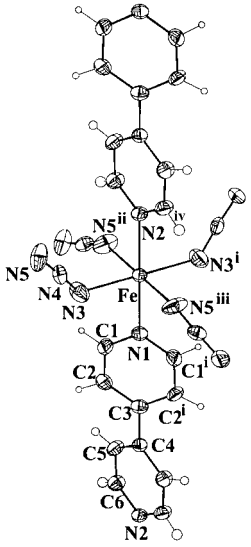

a)

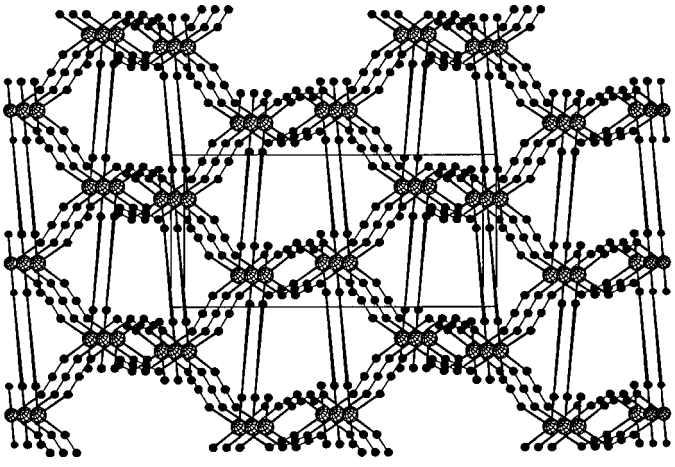

b)

Figure 4. a) Structural fragment showing the octahedral coordination environment around Fe and the atom-labeling scheme; b) 3D structure of [Fe(N_3)$_2$(4,4′-bpy)] (**II**) with all 4,4′-bpy ligands represented by black sticks.

The $M(H)$ data measured at 2 K on a random-oriented powder sample of **I** are shown in Figure 7. The sample was first cooled to 2 K in a zero magnetic field, then a measurement was made with a sequence of $0\rightarrow 54$ kG $\rightarrow 0\rightarrow -54$ kG $\rightarrow 0\rightarrow 54$ kG. A clear slope change is evident in the first ramping-up curve (data with triangles) at about $H_C=25$ kG, and this indicates a metamagnetic transition. At fields below H_C, the $M(H)$ data are that of a typical antiferromagnet. At fields higher than H_C, all Fe^{2+} moments are turned to the direction of the magnetic field. This initiates a large saturation moment of more than $2\mu_B$ per Fe^{2+}, and the system behaves like that of a soft ferromagnet. The ramping-down data, and the data in the loop with negative fields, reflect this change. The $M(H)$ of the second ramping-up curve (data with solid circles) does not repeat that of the first. Instead, it follows closely the data of the ramping-down curve, consistent with the behavior of a metamagnet.

Figure 8 shows the $M(H)$ data measured on a field aligned sample of **I**, with a field parallel to the easy direction. In contrast to $M(H)$ of the randomly oriented sample, $M(H)$ of this aligned sample in the easy direction behaves much like that of a hard magnet. A very large coercivity ($H_{coe}=34$ kG) is demonstrated, and this indicates a very large anisotropic energy is present in this compound. To the best of our knowledge, such a large hysteresis effect has not been observed before in molecular magnetic systems. The magnetization reaches $2.15\mu_B$ per Fe^{2+} at $H=250$ kG.

In Figure 9 we present ZFC and FC (field-cooled) χT data for **II**, measured with a very small applied field of 0.5 ± 0.5 G. The sudden increase of χT below 20 K indicates the existence of a spontaneous ferromagnetic ordering in this compound.

  0947-6539/02/0810-2242 $ 20.00+.50/0 *Chem. Eur. J.* **2002**, *8*, No. 10

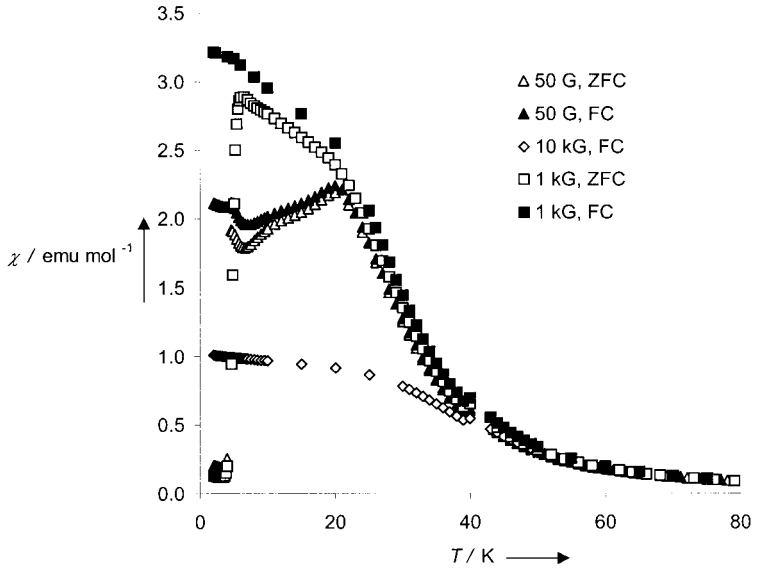

Figure 6. χT versus T data measured with applied fields of 50 G (triangles), 1 kG (squares), and 10 kG (diamonds) for 2D-[Fe$(N_3)_2$(4,4′-bpy)] (**I**).

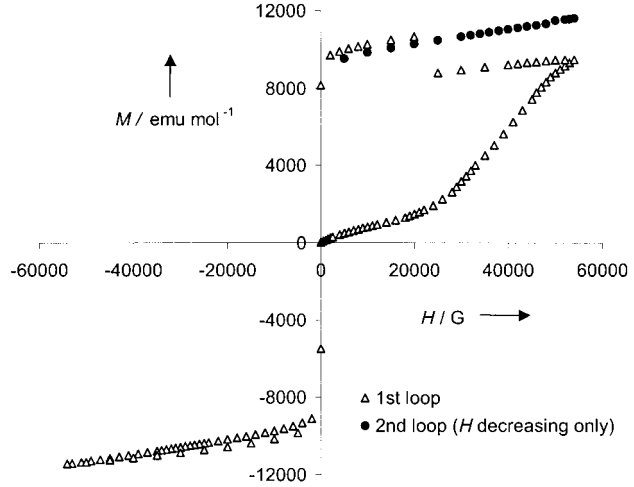

Figure 7. $M(H)$ versus H measured at 2 K for a randomly oriented powder sample of 2D-[Fe$(N_3)_2$(4,4′-bpy)] (**I**).

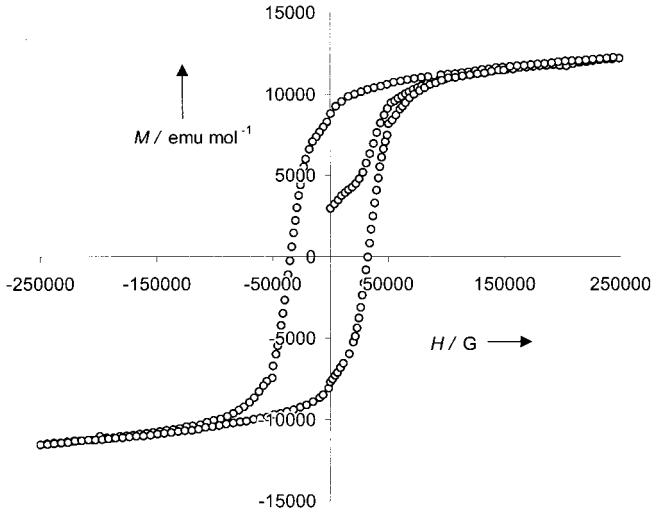

Figure 8. $M(H)$ versus H measured at 2 K for a field aligned sample of 2D-[Fe$(N_3)_2$(4,4′-bpy)] (**I**). The applied field in the measurement was in the easy direction.

The curves of χT versus T, measured under several higher fields, behave very similarly to that of 0.5 G, except for the less sharp data around the transition temperature, with the fact that the higher the field, the rounder the data curve towards the higher temperatures. This is typical behavior of a ferromagnet. Plotted as $1/\chi T$ versus T, the susceptibility data measured at 500 G, 1 kG, and 10 kG are also presented in Figure 9 as an insert. For the temperature above 40 K, these curves can be well fitted with the Curie–Weiss law $C/(T-\theta)$. The effective paramagnetic moment μ_{eff} and the Curie–Weiss temperature θ yielded from fitting, are $4.9\mu_B$ and -26 K, respectively.

The negative sign for θ, as seen clearly in the insert of Figure 9, suggests an overall antiferromagnetic coupling between the Fe^{2+} moments at temperatures above 40 K. This seems in contradiction to the observed ferromagnetic ordering below 20 K in the system. Nonetheless, the antiferromagnetic nature of the Fe^{2+} interaction at high temperature is also evidenced in the χT versus T plot shown in Figure 10 and its insert. As temperature T is lowered, the χT data decrease from $\approx 3\,\text{emu}\,\text{K}^{-1}\,\text{mol}^{-1}$ at room temperature, which is expected for a free Fe^{2+}, to a minimum of $\approx 2\,\text{emu}\,\text{K}^{-1}\,\text{mol}^{-1}$ at $T = 31$ K. Such variation of χT versus T is expected for an antiferromagnetic coupling. However, as T is further decreased from 31 K, which is still well above T_C of 20 K, χT starts to increase, until it reaches its maximum value at ≈ 16 K. χT decreases as T decreases from 16 to 0 K, due to the Fe^{2+} saturation at low T. The increase in χT upon cooling in the $16\,\text{K} < T < 31\,\text{K}$ range indicates that a positive exchange coupling of Fe^{2+} is dominant at temperatures below 31 K, and it could be responsible for the ferromagnetic-like phase transition at 20 K. A similar change in sign for the exchange coupling from "$-$" at high T to "$+$" at low T was previously observed in the isostructural compound [Mn(4,4′-bpy)$(N_3)_2]_n$[16, 17] and in two other metal–azido networks with 2D networks, [Mn(4-acpy)$_2(N_3)_2]_n$[18] and [Mn(py)$_2(N_3)_2]_n$.[7d] However, the turning points for χT in these systems are all very close to the transition temperatures of the long-range magnetic ordering characterized as an antiferromagnetic kind with canting phenomena. This is very different from what is observed in our 3D-[Fe$(N_3)_2$(4,4′-bpy)] system, that is, the turning point for χT is at 31 K, 11 K higher than T_C.

Figure 11 illustrates the $M(H)$ data measured at 2 K on **II**. In the low-field region, the $M(H)$ curve behaves somewhat like a ferromagnet. A noticeable hysteresis loop is observed as shown in the insert of Figure 11. The coercivity is found to be $H_{\text{coe}} = 900$ G, much smaller than that of **I**. The $M(H)$ value continues to increase with a rather large slope, as the field

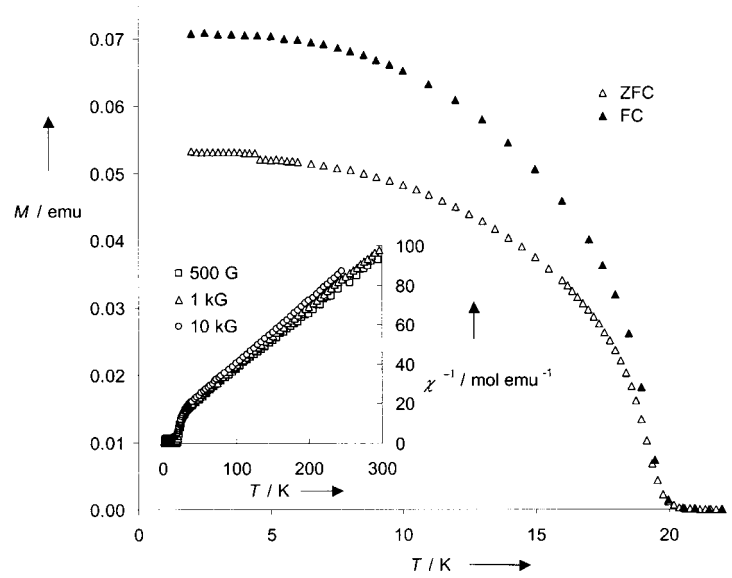

Figure 9. $M(T)$ versus T measured in an applied field of 0.5 G on a powder sample of 3D-[Fe(N_3)$_2$(4,4′-bpy)] (**II**). The empty triangles are the zero-field-cooled (ZFC) data, and the solid triangles are the field-cooled (FC) data. The insert shows $1/\chi$ versus T data measured with an applied field of 500 G (squares), 1 kG (triangles), and 10 kG (circles).

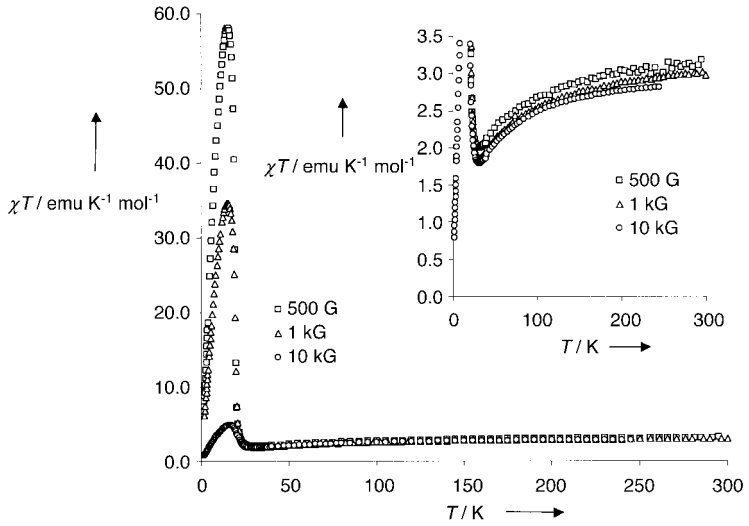

Figure 10. χT versus T data of 500 G (squares), 1 kG (triangles), and 10 kG (circles) for 3D-[Fe(N_3)$_2$(4,4′-bpy)] (**II**). The insert is a blowup in the lower temperature region.

increases from 30 kG and above. At the largest field of 250 kG, $M(H)$ reaches 13×10^3 emu mol^{-1}, which is 2.33μ_B per Fe^{2+}, a little less than half of the μ_{eff} for Fe^{2+} at the high temperatures. Possible existence of a large anisotropy energy in this compound may be considered for the explanation of the nonsaturation behavior of the $M(H)$ curve. In contrast to $M(H)$ of the isostructral compound [Mn(4,4′-bpy)(N_3)$_2$]$_n$, for which a canting antiferromagnetic structure that produces weak ferromagnetism was proposed, the $M(H)$ of 3D-[Fe(N_3)$_2$(4,4′-bpy)] is very suggestive that the ground state magnetic structure of it is ferromagnetic. Yet, we could not exclude the possibility that such behavior is due to the fact that the ground state magnetic structure is not a truly ferromagnetic one. In other words, there could exist a certain kind of canting structure that would produce a ferromagnetic component in a particular direction, though for most of the cases involving canting phenomena, the $M(H)$ values would not reach as high as that of 3D-[Fe(N_3)$_2$(4,4′-bpy)].

The data of molar heat capacity $C(T)$ measured in zero field and a field of 35 kG are presented in Figure 12. A cusp-like anomaly with a peak value of 32 J mol^{-1} K^{-1} at $T = 20$ K is clearly seen for the zero-field $C(T)$ data set, consistent with the spontaneous ferromagnetic phase transition observed in the χT measurements. The Curie temperature T_C, determined from $C(T)$ measurements, is consistent with that determined from the χT measurements. In the $C(T)$ of the 35 kG data set, the peak is shifted to 21.5 K, and the anomaly is spread out to a much wider range of T. The shift towards to a higher temperature of the $C(T)$ anomaly under an applied field is typical for ferromagnetic systems, thus the result of $C(T)$ measurements supports strongly the ferromagnetic ground state exhibited in **II**. Due to a lack of knowledge on the phonon contribution to the total heat capacity, magnetic entropy removal ΔS_m was estimated by integrating $\Delta C(T)/T$ versus T curve from 15 to 21.5 K, in which $\Delta C(T)$ is the difference between the measured $C(T)$ curve and a smooth curve $C'(T)$, obtained by extrapolating the $C(T)$ data at far below, and far above the anomalous region. The estimated ΔS_m is 3.2 J mol^{-1} K^{-1}, which is about 24 % of 13.5 J mol^{-1} K^{-1}, a value calculated from $\Delta S_{calcd} = Nk_B \ln(2S+1)$, assuming $S = 2$ for free Fe^{2+}. It is also interesting to note that the shape of the zero-field $C(T)$ anomaly is not that of a typical second-order transition, in that the slopes on both sides of the cusp are rather symmetric, which is different from the asymmetric, λ-like shape predicted by a mean-field theory. Further investigations are on the way to see whether a crystalline structure transformation also occurs in the vicinity of T_C, participating in the overall $C(T)$ anomaly, in addition to the anomaly originating from the magnetic phase transition.

The magnetic interactions of Fe^{2+} in the 3D-[Fe(N_3)$_2$(4,4′-bpy)] network are achieved mainly through the μ-(1,3) bridging azido ligands. Because the μ-(1,3) bridging is

  0947-6539/02/0810-2244 $ 20.00+.50/0 *Chem. Eur. J.* **2002**, *8*, No. 10

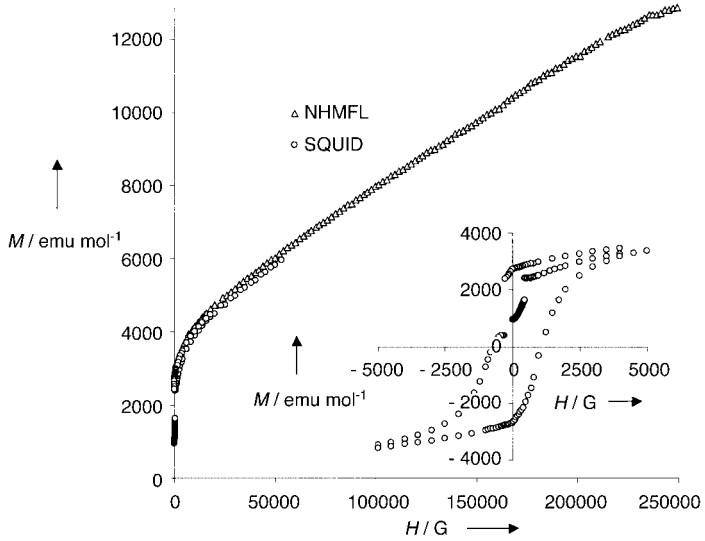

Figure 11. $M(H)$ versus H measured at 2 K for 3D-[Fe(N$_3$)$_2$(4,4′-bpy)] (**II**). The circles are the data measured by using an in-house SQUID magnetometer. The triangles are the data measured by using a vibration-sample magnetometer in a 30-tesla magnet at the National High Magnetic Field Laboratory (NHMFL). Shown in the insert are the data of a 2 K hysteresis-loop measurement.

expected to be antiferromagnetic, the unique network of 3D-[Fe(N$_3$)$_2$(4,4′-bpy)] involving the two types of helical pathways would produce a very interesting arrangement for the Fe^{2+} moments when ordered: for the Fe^{2+} lining along both [010] (the direction for both helices) and [100] direction, their moments would have to be oriented in the same direction, or at least a component of their moments would be in the same direction. In effect, this would be true for the Fe^{2+} moments lining along the 4,4′-bpy molecular axis as well. The complex antiferro–ferromagnetic magnetic correlation observed in both [Mn(4,4′-bpy)(N$_3$)$_2$]$_n$ and 3D-[Fe(N$_3$)$_2$(4,4′-bpy)] systems may have originated from this topological uniqueness. However, this alone cannot explain the overwhelming ferromagnetic interaction of the Fe^{2+}, which leads to the long-range ferromagnetic ordering with rather high T_C in the 3D-[Fe(N$_3$)$_2$(4,4′-bpy)] system, in contrast to the weak ferromagnetic behavior exhibited in the Mn isostructural compound. Orbital contribution to the Fe^{2+} moment, especially at low temperatures, should be considered because of the distorted octahedral environment of iron. Low-temperature structural information will also be crucial. Our ongoing investigations using complementary experimental techniques will further reveal the true nature of the magnetic ordering of this compound.

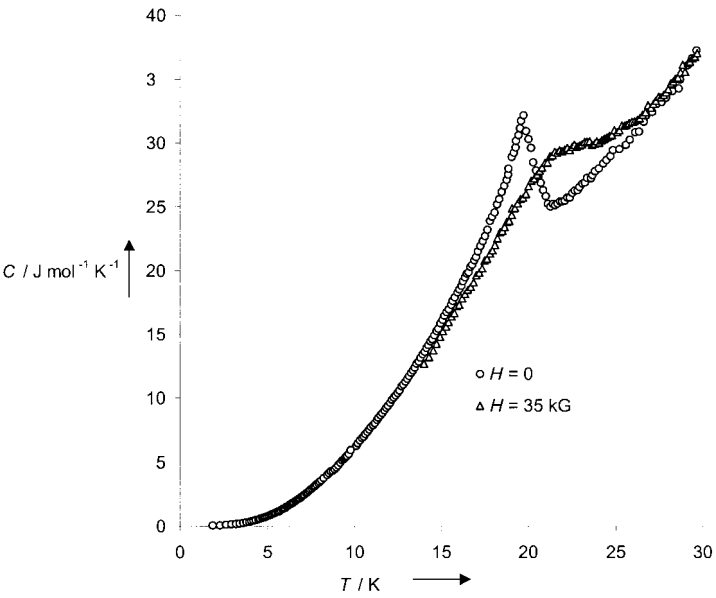

Figure 12. Specific heat $C(T)$, defined as molar heat capacity measured in zero field (circles) and a field of 35 kG (triangles) for 3D-[Fe(N$_3$)$_2$(4,4′-bpy)] (**II**).

Conclusion

Single crystals of 2D-[Fe(N$_3$)$_2$(4,4′-bpy)] and 3D-[Fe(N$_3$)$_2$(4,4′-bpy)] were obtained using a diffusion method. Phase-pure samples of both compounds were synthesized by optimal solution reactions. Different coordination modes of azido bridges, end-on (EO) in **I** and end-to-end (EE) in **II**, induced different magnetic coupling in the two compounds. The 2D-[Fe(N$_3$)$_2$(4,4′-bpy)] (**I**) represents another member of the [ML$_2$(4,4′-bpy)] series. The magnetic properties of 2D-[Fe(N$_3$)$_2$(4,4′-bpy)] are similar to those of metamagnets [MCl$_2$(4,4′-bpy)], except that the critical-field H_C and the coercivity H_{coe} for 2D-[Fe(N$_3$)$_2$(4,4′-bpy)] (**I**) is much larger. The low-temperature magnetic behavior of 3D-[Fe(N$_3$)$_2$(4,4′-bpy)] (**II**) is that of a ferromagnet, in contrast to that of isostructural [Mn(N$_3$)$_2$(4,4′-bpy)]. The dominant exchange coupling of Fe^{2+} in **I** is ferromagnetic, as expected for the μ-(1,1) bridging by the azide unit. However, the exchange coupling of Fe^{2+} in **II** changes sign from negative at high temperature (consistent with the predicted antiferromagnetic coupling by μ-(1,3) azido bridging), to positive at low temperature, which leads to the long-range ferromagnetic ordering. Further investigations will contribute to a better understanding of the structure–property correlation and its origin in these and related compounds.

Experimental Section

Chemicals and reagents: All chemicals used were as purchased without purification: FeCl$_2$·4H$_2$O (99+%, Acros), FeSO$_4$·7H$_2$O (Analytical Reagent, Mallinckrodt), NaN$_3$ (99%, Alfa Aesar), 4,4′-bipyridine (98%, Alfa Aesar), and methanol (99.9%, Fisher).

Synthesis of 2D-[Fe(N$_3$)$_2$(4,4′-bpy)] (I): Plum plate crystals of **I** were obtained from a diffusion reaction in a U-tube with ethylene glycol as diffusion mediate. An aqueous solution (3 mL) of FeCl$_2$·4H$_2$O (0.01988 g, 0.1 mmol) was added to the left side of the diffusion tube. A mixture of a solution of 4,4′-bpy in methanol (1 mL, 0.1M) and an aqueous solution of NaN$_3$ (2 mL, 0.1M) was added to the right side. The tube was then left at room temperature for one month, with the opening of both sides covered by parafilm. A pure powder sample of **I** was prepared by quickly mixing a solution of 4,4′-bpy in methanol (10 mL, 0.1M) with an aqueous solution (20 mL) of FeCl$_2$·4H$_2$O (0.1988 g, 1 mmol), followed by addition of an aqueous solution of NaN$_3$ (20 mL, 0.1M). Brown powder of **I** was filtered out and collected (153 mg, yield 52%) after the beaker was placed at room temperature for 20 hours with the opening covered by parafilm.

Synthesis of 3D-[Fe(N$_3$)$_2$(4,4′-bpy)] (II): Deep red polyhedral crystals of **II** were grown from the same reaction as described above for **I**. A pure

powder sample of **II** was obtained by slowly adding a solution of 4,4′-bpy in methanol (10 mL, 0.1M) to a stirred aqueous solution (20 mL) of $FeCl_2 \cdot 4H_2O$ (0.1988 g, 1 mmol), or $FeSO_4 \cdot 7H_2O$ (0.2780 g, 1 mmol). Then, an aqueous solution of NaN_3 (20 mL, 0.1M) was added dropwise. The stirring was continued for three hours under ambient conditions. A deep red powder of **II** was then filtered out and collected (44%) after the beaker was placed at room temperature for 29 hours, with the opening covered by parafilm.

Crystallographic studies: A plum column crystal of **I** with approximate dimensions $0.22 \times 0.10 \times 0.01$ mm^3, and a deep red crystal of **II** with approximate dimensions $0.20 \times 0.20 \times 0.10$mm^3, were mounted on glass fibers in air and used for crystal structure analysis on an Enraf-Nonius CAD4 automated diffractometer. Twenty reflections for **I** and twenty five reflections for **II** were centered by using graphite monochromated $Mo_{K\alpha}$ radiation. Crystal data were collected with the ω-scan technique, within the limits of $3.56^\circ < \theta < 24.99^\circ$ for **I** and $2.79^\circ < \theta < 25.95^\circ$ for **II** at 293 ± 1 K. Intensity values were corrected for Lorentz and polarization effects, and an empirical absorption correction based on ψ-scan data[19] was applied in each case. The structures were solved by using the SHELX-97 program.[20] Non-hydrogen atoms were located by direct phase determination and subjected to anisotropic refinement. For **I**, the hydrogen atoms were determined theoretically, while for **II**, the hydrogen atoms were located from a difference Fourier map and refined isotropically. The unit cell parameters, along with data collection and refinement details for **I** and **II**, are shown in Table 1. Final atomic coordinates and isotropic thermal parameters are given in Tables 2 and 3. Selected bond lengths and angles are presented in Tables 4 and 5. The structural factors and anisotropic displacement parameters were deposited at CCDC. Crystal drawings were generated by SCHAKAL 97.[21]

Table 1. Crystallographic data for **I** and **II**.

	I	**II**
empirical formula	$C_{10}H_8FeN_8$	$C_{10}H_8FeN_8$
M_w	296.09	296.09
space group	*Cmmm* (No. 65)	$P4_12_12$ (No. 92)
a [Å]	11.444(2)	8.132(1)
b [Å]	15.181(3)	8.132(1)
c [Å]	3.458(1)	16.708(3)
V [Å^3]	600.8(2)	1104.9(3)
Z	2	4
T [K]	293 ± 1	293 ± 1
λ [Å]	0.71073	0.71073
ρ_{calcd} [g cm^{-3}]	1.637	1.780
μ [mm^{-1}]	1.254	1.364
R[a] [$I > 2\sigma(I)$]	0.0725	0.0408
R_w[b]	0.1454	0.0856

[a] $R1 = \frac{\sum \| F_o| - |F_c \|}{\sum |F_o|}$. [b] $wR2 = \sqrt{\frac{\sum [w(F_o^2 - F_c^2)^2]}{\sum w(F_o^2)^2}}$ and $\mathrm{Goof} = S = \sqrt{\frac{\sum [w(F_o^2 - F_c^2)^2]}{n - p}}$.

Table 2. Atomic coordinates and equivalent isotropic temperature factors [Å^2] for **I**.

Atoms	x	y	z	U_{eq}[a]
Fe	0	0.5000	0.5000	0.034(1)
N1	0.1916(10)	0.5000	0.5000	0.033(3)
N2	0	0.4095(6)	0	0.034(3)
N3	0	0.3341(7)	0	0.058(4)
N4[b]	0.0350(6)	0.2590(10)	0	0.100(3)
C1	0.2505(11)	0.4272(6)	0.5000	0.061(3)
C2	0.3714(11)	0.4238(6)	0.5000	0.065(4)
C3	0.4344(12)	0.5000	0.5000	0.031(3)
H1	0.2094	0.3743	0.5000	0.074
H2	0.4096	0.3697	0.5000	0.078

[a] U_{eq} defined as one third of the trace of the orthogonalized **U** tensor. [b] N4 atoms are half occupied.

Table 3. Atomic coordinates and equivalent isotropic temperature factors [Å^2] for **II**.

Atoms	x	y	z	U_{eq}[a]
Fe	0.2910(1)	0.2910(1)	0	0.022(1)
N1	0.4812(4)	0.4812(4)	0	0.026(1)
N2	1.0971(4)	1.0971(4)	0	0.025(1)
N3	0.4222(5)	0.1603(5)	0.0907(2)	0.045(1)
N4	0.3799(4)	0.0430(5)	0.1263(2)	0.030(1)
N5	0.3460(5)	−0.0745(5)	0.1607(3)	0.047(1)
C1	0.6417(5)	0.4439(5)	−0.0008(4)	0.031(1)
C2	0.7642(5)	0.5582(5)	−0.0009(3)	0.029(1)
C3	0.7235(5)	0.7235(5)	0	0.026(1)
C4	0.8535(5)	0.8535(5)	0	0.023(1)
C5	1.0036(6)	0.8290(5)	−0.0375(3)	0.030(1)
C6	1.1189(5)	0.9519(6)	−0.0360(3)	0.030(1)
H1	0.6640(4)	0.3320(4)	0.0030(2)	0.015(8)
H2	0.8690(4)	0.5200(4)	0.0050(2)	0.017(9)
H3	1.0450(5)	0.7360(5)	−0.0570(2)	0.030(12)
H4	1.2090(6)	0.9340(6)	−0.0650(3)	0.048(14)

[a] U_{eq} defined as one third of the trace of the orthogonalized **U** tensor.

Table 4. Selected bond lengths [Å] and bond angles [°] for **I**.[a]

Fe–N1	2.192(11)	N2–N3	1.146(12)
Fe–N1^{i}	2.192(11)	N2–Fe^{v}	2.208(6)
Fe–N2	2.208(6)	N3–N4^{vi}	1.21(3)
Fe–N2^{i}	2.208(6)	N3–N4	1.21(3)
Fe–N2^{ii}	2.208(6)	Fe–N2^{iii}	2.208(6)
N1–Fe–N1^{i}	180.0	N2^{ii}–Fe–N2^{iii}	180.0
N1–Fe–N2	90.0	N1^{i}–Fe–N2	90.0
N1–Fe–N2^{i}	90.0	N1^{i}–Fe–N2^{i}	90.0
N2^{i}–Fe–N2^{ii}	76.9(4)	N3–N2–Fe	128.46(18)
N2–Fe–N2^{i}	180.0	N3–N2–Fe^{v}	128.46(18)
N1–Fe–N2^{ii}	90.0	Fe–N2–Fe^{v}	103.1(4)
N1^{i}–Fe–N2^{ii}	90.0	N2–N3–N4^{vi}	160(3)
N2–Fe–N2^{ii}	103.1(4)	N2–N3–N4	160(3)
N1–Fe–N2^{iii}	90.0	N1^{i}–Fe–N2^{iii}	90.0
N2–Fe–N2^{iii}	76.9(4)	N2^{i}–Fe–N2^{iii}	103.1(4)

[a] Symmetry transformations used to generate equivalent atoms: i $-x, -y+1, -z+1$, ii $x,y,z+1$, iii $-x, -y+1, -z$, iv $x, -y+1,z$, v $x,y,z-1$, vi $-x,y, -z$.

Table 5. Selected bond lengths [Å] and bond angles [°] for **II**.[a]

Fe–N3^{i}	2.136(4)	N3–N4	1.176(5)
Fe–N3	2.136(4)	N4–N5	1.148(5)
Fe–N5^{ii}	2.160(4)	N5–Fe^{vi}	2.160(4)
Fe–N5^{iii}	2.160(4)	Fe–N1	2.188(4)
Fe–N2^{iv}	2.230(4)	N2–Fe^{v}	2.230(4)
N3^{i}–Fe–N3	179.8(3)	N3^{i}–Fe–N5^{ii}	91.11(15)
N3–Fe–N5^{ii}	88.89(15)	N3^{i}–Fe–N5^{iii}	88.89(15)
N3–Fe–N5^{iii}	91.11(15)	N4–N3–Fe	128.1(3)
N5^{ii}–Fe–N5^{iii}	179.3(2)	N5–N4–N3	176.8(5)
N3^{i}–Fe–N1	89.92(12)	N4–N5–Fe^{vi}	153.0(4)
N3–Fe–N1	89.92(12)	N1–Fe–N2^{iv}	180.00(17)
N5^{ii}–Fe–N1	90.37(12)	N5^{iii}–Fe–N1	90.37(12)
N3^{i}–Fe–N2^{iv}	90.08(12)	N3–Fe–N2^{iv}	90.08(12)
N5^{ii}–Fe–N2^{iv}	89.63(12)	N5^{iii}–Fe–N2^{iv}	89.63(12)

[a] Symmetry transformations used to generate equivalent atoms: i $y,x, -z$, ii $y+1/2, -x+1/2,z-1/4$, iii $-x+1/2,y+1/2, -z+1/4$, iv $x-1,y-1,z$, v $x+1,y+1,z$, vi $-y+1/2,x-1/2,z+1/4$.

X-ray powder diffraction analyses were performed on a Rigaku D/M-2200T automated diffraction system (Ultima$^+$). The measurements were made with a 2θ range between 5 and 80°, at the operation power of 40 KV/40 mA. X-ray powder diffraction analyses were used for phase identification.

CCDC-171656 (**I**) and CCDC-171657 (**II**) contain the supplementary crystallographic data for this paper. These data can be obtained free of

0947-6539/02/0810-2246 $ 20.00+.50/0 *Chem. Eur. J.* **2002**, *8*, No. 10

charge via www.ccdc.cam.ac.uk/conts/retrieving.html (or from the Cambridge Crystallographic Data Centre, 12 Union Road, Cambridge CB21EZ, UK; fax: (+44) 1223-336-033; or e-mail: deposit@ccdc.cam.uk).

Magnetic measurements: Magnetic susceptibility and field- (H) dependent magnetization measurements up to $H = 5.4$ T were performed by using a Quantum Design SQUID magnetometer. These measurements included the field-dependent magnetization, $M(H)$, at several temperatures and magnetic susceptibility, χT, under a number of applied magnetic fields. χT is defined as $M(T)/H$, in which $M(T)$ is the temperature-dependent magnetization. χT of different fields was measured from 2 to 350 K. Both zero-field-cooled (ZFC) and field-cooled (FC) measurements were performed for each sample. The applied magnetic field H for the $M(H)$ measurements was increased from 0 to 5.4 T and then decreased back to 0 T. In the hysteresis measurements, H was varied according to the following: $H = 0 \rightarrow H_{max} \rightarrow 0 \rightarrow -H_{max} \rightarrow 0 \rightarrow H_{max}$.

High-field M(H) measurements ($H_{max} = 30$ T) at $T = 2$ K were performed at the National High Magnetic Field Lab, Tallahassee, by using a Lakeshore Vibration Sample Magnetometer with a 33-tesla magnet. For **I**, $M(H)$ was measured on polycrystalline powder samples with random orientation (powder pressed into a pellet), and with field aligned orientation. The field-aligned sample was prepared by using a process, in which the sample powder was mixed with 30-minute epoxy, then cured at room temperature in a high magnetic field of 20 tesla. For **II**, $M(H)$ was measured only on powder samples with random orientation.

Acknowledgements

The generous support from the National Science Foundation with Grants DMR-9553066 and DMR-9633018, and the support from the National High Magnetic Field Laboratory are gratefully acknowledged.

[1] a) O. Kahn, *Molecular Magnetism*, WILEY-VCH, New York, **1993**; b) G. De Munno, R. Ruiz, F. Lloret, R. Sessoli, M. Julve, *Inorg. Chem.* **1995**, *34*, 408; c) S. Turner, O. Kahn, L. Rabardel, *J. Am. Chem. Soc.* **1996**, *118*, 6428; d) N. L. Frank, R. Clerac, J.-P. Sutter, N. Daro, O. Kahn, C. Coulon, M. T. Green, S. Golhen, L. Ouahab, *J. Am. Chem. Soc.* **2000**, *122*, 2053; e) O. Kahn, *Acc. Chem. Res.* **2000**, *33*, 647; f) J. S. Miller, J. L. Manson, Q.-Z. Huang, J. W. Lynn, H.-J. Koo, M.-H. Whangbo, R. Bateman, T. Otsuka, N. Wada, D. N. Argyriou, *J. Am. Chem. Soc.* **2000**, *123*, 162; g) D. C. Gordon, L. Deakin, A. M. Arif, J. D. Miller, *J. Am. Chem. Soc.* **2000**, *122*, 290.

[2] a) J. Y. Lu, M. A. Lawandy, J. Li, T. Yuen, C. L. Lin, *Inorg. Chem.* **1999**, *38*, 2695; b) M. A. Lawandy, X. Huang, R. Wang, J. Li, J. Y. Lu, T. Yuen, C. Lin, *Inorg. Chem.* **1999**, *38*, 5410.

[3] a) J. L. Manson, A. M. Arif, J. S. Miller, *Chem. Commun.* **1999**, 1479; b) M. A. S. Goher, F. A. Mautner, *Polyhedron* **1998**, *17*, 1561; c) G. D. Munno, M. Julve, G. Viau, F. Lloret, J. Faus, D. Viterbo, *Angew. Chem.* **1996**, *108*, 1931; *Angew. Chem. Int. Ed. Engl.* **1996**, *35*, 1807; d) Z. E. Serna, M. G. Barandika, R. Cortés, M. K. Vrtiaga, G. E. Barberis, T. Rojo, *Dalton* **2000**, 29; e) X. Hao, Y. Wei, S. Zhang, *Chem. Commun.* **2000**, 2271.

[4] a) A. Escuer, I. Castro, F. Mautner, M. S. E. Fallah, R. Vicente, *Inorg. Chem.* **1997**, *36*, 4633; b) A. Escuer, R. Vicente, M. A. S. Goher, F. A. Mautner, *J. Chem. Soc. Dalton Trans.* **1997**, 4431; c) R. Vicente, A. Escuer, *Polyhedron* **1995**, *14*, 2133.

[5] a) J. Lorösch, H. Paulus, W. Haase, *Inorg. Chim. Acta* **1985**, *106*, 101; b) M. A. Goher, T. C. W. Mak, *Inorg. Chim. Acta* **1985**, *99*, 223.

[6] a) A. Escuer, M. Font-Bardia, E. Peñalba, X. Solans, R. Vicente, *Polyhedron* **1998**, *18*, 211; b) G. De Munno, J. A. Real, M. Julve, M. C. Muñoz, *Inorg. Chim. Acta* **1993**, *211*, 227; c) M. A. S. Goher, H. J. Wang, T. C. W. Mark, *J. Mol. Struct.* **1991**, *242*, 179.

[7] a) R. Gortés, M. Drillon, X. Solans, L. Lezama, T. Rojo, *Inorg. Chem.* **1997**, *36*, 677; b) M. A. M. Abu-Youssef, A. Escuer, M. A. S. Goher, F. A. Mautner, G. J. Reiß, R. Vicente, *Angew. Chem.* **2000**, *112*, 1681; *Angew. Chem. Int. Ed.* **2000**, *39*, 1624; c) H. Shen, W. Bu, E. Gao, D. Liao, Z. Jiang, S. Yan, G. Wang, *Inorg. Chem.* **2000**, *39*, 396; d) A. Escuer, R. Vicente, M. A. S. Goher, F. A. Mautner, *Inorg. Chem.* **1997**, *36*, 3440; e) M. Monfort, I. Resino, J. Ribas, H. Stoeckli-Evans, *Angew. Chem.* **2000**, *112*, 197; *Angew. Chem. Int. Ed.* **2000**, *39*, 191; f) M. A. Youssef, A. Escuer, M. A. S. Goher, F. A. Mautner, R. Vicente, *Dalton* **2000**, 413; g) G. Viau, M. G. Lombardi, G. D. Munno, M. Julve, F. Lloret, J. Faus, A. Ganeschi, J. M. Clemente-Juan, *Chem. Commun.* **1997**, 1195.

[8] a) S. Wang, L. Wang, X. Wang, Q. Luo, *Inorg. Chim. Acta* **1997**, *254*, 71; b) M. K. Ellison, H. Nasri, Y. Xia, J. Marchon, C. E. Schulz, P. G. Debrunner, W. R. Scheidt, *Inorg. Chem.* **1997**, *36*, 4804.

[9] a) C. S. Hong, Y. Do, *Angew. Chem.* **1999**, *111*, 153; *Angew. Chem. Int. Ed.* **1999**, *38*, 193; b) L. K. Thompson, S. S. Tandon, *Comments Inorg. Chem.* **1996**, *18*, 125; c) M. F. Charlot, O. Kahn, M. Chaillet, C. Larrien, *J. Am. Chem. Soc.* **1986**, *108*, 2574; d) M. A. Aebersold, B. Gillon, D. Plantevin, O. Kahn, *J. Am. Chem. Soc.* **1998**, *120*, 5238; e) R. Cortés, L. Lezama, J. L. Pizarro, M. I. Arriortua, X. Solans, T. Rojo, *Angew. Chem.* **1994**, *106*, 2520; *Angew. Chem. Int. Ed. Engl.* **1994**, *33*, 2488; f) R. Cortés, L. Lezama, J. L. Pizarro, M. I. Arriortua, X. Solans, T. Rojo, *Angew. Chem.* **1994**, *106*, 2520; *Angew. Chem. Int. Ed. Engl.* **1994**, *33*, 2488; g) J. Ribas, M. Monfort, C. Diaz, C. Bastos, X. Solans, *Inorg. Chem.* **1993**, *32*, 3557; h) R. Cortés, J. L. Pizarro, L. Lezama, M. I. Arriortua, T. Rojo, *Inorg. Chem.* **1994**, *33*, 2697; i) R. Cortés, M. Drillon, X. Solans, L. Lezama, T. Rojo, *Inorg. Chem.* **1997**, *36*, 677; j) G. D. Munno, T. Poerio, G. Viau, M. Julve, G. Lloret, *Angew. Chem.* **1997**, *109*, 1531; *Angew. Chem. Int. Ed. Engl.* **1997**, *36*, 1459; k) C. G. Pierpont, D. N. Hendrickson, D. M. Duggan, F. Wagner, E. K. Barefield, *Inorg. Chem.* **1975**, *14*, 604; l) A. Escuer, R. Vicente, J. Ribas, M. S. El Fallah, X. Solans, M. Font-Bardia, *Inorg. Chem.* **1993**, *32*, 3727; m) R. Cortés, M. K. Vrtiaga, L. Lezama, J. L. Pizarro, A. Goñi, M. I. Arriortua, T. Rojo, *Inorg. Chem.* **1994**, *33*, 4009; n) L. K. Thompson, S. S. Tandon, M. E. Manuel, *Inorg. Chem.* **1995**, *34*, 2356; o) R. Cortés, L. Lezama, J. L. Pizarro, M. I. Arriortua, T. Rojo, *Angew. Chem.* **1996**, *108*, 1934; *Angew. Chem. Int. Ed. Engl.* **1996**, *35*, 1810; p) E. Ruiz, J. Cano, S. Alvarez, P. Alemany, *J. Am. Chem. Soc.* **1998**, *120*, 11122; q) F. A. Mautner, R. Cortés, L. Lezama, T. Rojo, *Angew. Chem.* **1996**, *108*, 96; *Angew. Chem. Int. Ed. Engl.* **1996**, *35*, 78.

[10] a) P. J. Haguman, D. Hagrman, J. Zubieta, *Angew. Chem.* **1999**, *111*, 2798; *Angew. Chem. Int. Ed.* **1999**, *38*, 2638; b) S. R. Batten, R. Robson, *Angew. Chem.* **1998**, *110*, 1558; *Angew. Chem. Int. Ed.* **1998**, *37*, 1460; c) O. M. Yaghi, H. Li, C. Davis, D. Richardson, T. L. Groy, *Acc. Chem. Res.* **1998**, *31*, 474.

[11] L. Pan, N. Zheng, Y. Wu, X. Jing, X. Huang, *J. Coord. Chem.* **1999**, *47*, 269.

[12] M. L. Hernández, M. G. Barandika, M. K. Urtiaga, R. Cortés, L. Lezama, M. I. Arriortua, *Dalton* **2000**, 79.

[13] G. O. Munno, M. Julve, G. Viau, F. Lloret, J. Faus, D. Viterbo, *Angew. Chem.* **1996**, *108*, 1931; *Angew. Chem. Int. Ed. Engl.* **1996**, *35*, 1807.

[14] a) M. L. Hernández, M. G. Barandika, M. K. Urtiaga, R. Cortés, L. Lezama, M. Z. Arriortua, T. Rojo, *J. Chem. Soc. Dalton Trans.* **1999**, 1401; b) K. R. Reddy, M. V. Rajasekharan, J.-P. Tuchagues, *Inorg. Chem.* **1998**, *37*, 5978; c) G. D. Munno, T. Poerio, G. Viau, M. Julve, F. Lloret, Y. Journaur, E. Rivière, *Chem. Commun.* **1996**, 2587; d) K. Meyer, E. Bill, B. Mienert, T. Weyhermüller, K. Wieghardt, *J. Am. Chem. Soc.* **1999**, *121*, 4859; e) K. R. Reddy, M. V. Rajasekharan, J. P. Tuchagues, *Inorg. Chem.* **1998**, *37*, 5978.

[15] J. Ribas, A. Escuer, M. Monfort, R. Vicent, R. Cortés, L. Lezama, T. Rojo, *Coord. Chem. Rev.* **1999**, *193–195*, 1027.

[16] a) S. Han, J. L. Manson, J. Kim, J. S. Miller, *Inorg. Chem.* **2000**, *39*, 4182; b) C. M. Liu, R. G. Xiong, K. Liu, X. Z. You, *Inorg. Chem. Commun.* **1999**, 31; c) L. Pan, N. W. Zheng, Y. G. Wu, X. Y. Huang, *Chin. J. Struct. Chem.* **1999**, *18*, 41; d) H. Y. Shen, D. Z. Liao, Z. H. Jiang, S. P. Yan, B. W. Sun, G. L. Wang, X. K. Yao, H. G. Wang, *Chem. Lett.* **1998**, 469.

[17] R. Cortes, S. Martin, L. Lezama, G. Barandika, T. Rojo, J. L. Pizarro, *Proc. XXXIII ICCC* p. 352.

[18] A. Escuer, R. Vicente, M. A. S. Goher, F. A. Mautner, *Inorg. Chem.* **1995**, *34*, 5707.

[19] G. Kopfmann, R. Hubber, *Acta Crystallogr. Sect. A* **1968**, *24*, 348.

[20] G. M. Sheldrick, SHELX-97, Program for Structure Refinement, University of Göttingen, Göttingen (Germany), **1997**.

[21] E. Keller, SCHAKAL97, Computer Program for the Graphic Representation of Molecular and Crystallographic Models, University of Freiburg, Freiburg (Germany), **1997**.

Received: October 4, 2001 [F3591]